Light-quark mass dependence of the nucleon axial charge and pion-nucleon scattering phenomenology

Fernando Alvarado[*] and Luis Alvarez-Ruso[†]

Instituto de Física Corpuscular (IFIC) and Departamento de Física Teórica,
Consejo Superior de Investigaciones Científicas (CSIC) and Universidad de Valencia (UV),
E-46980 Paterna, Valencia, Spain

The light-quark mass dependence of the nucleon axial isovector charge (g_A) has been studied up to next-to-next-to-leading order, $\mathcal{O}(p^4)$, in relativistic chiral perturbation theory using extended-on-mass-shell renormalization, without and with explicit $\Delta(1232)$ degrees of freedom. We show that in the Δ-less case, at this order, the flat trend of $g_A(M_\pi)$ exhibited by state-of-the-art lattice QCD (LQCD) results cannot be reproduced using low energy constants extracted from pion-nucleon elastic and inelastic scattering. A satisfactory description of these LQCD data is only achieved in the theory with Δ. From this fit, we report $g_A(M_{\pi(\text{phys})}) = 1.260 \pm 0.012$, close to the experimental result, and $d_{16} = -0.88 \pm 0.88$ GeV^{-2}, in agreement with its empirical value. The large uncertainties are of theoretical origin, reflecting the difference between $\mathcal{O}(p^3)$ and $\mathcal{O}(p^4)$ that still persists at large M_π in presence of the Δ.

I. INTRODUCTION

The axial isovector charge g_A^{u-d} (g_A from now on) is a fundamental property of the nucleon related to the difference in the spin fractions carried by u and d quarks. With a magnitude precisely determined from neutron β decay,[1] the nucleon axial charge represents a benchmark for nonperturbative studies of quantum chromodynamics (QCD) in the lattice (LQCD) alongside with other nucleon properties, such as scalar and tensor charges, electromagnetic form factors, and parton distribution functions (see Ref. [3] and Sec. 10 of Ref. [4] for recent reviews). Over the last decade, progress in this direction has been significant [4], owing to better computational resources, improved algorithms, and techniques to reduce systematic errors, in particular, those induced by excited-state contamination, which can be considerable in the baryon sector for currently available lattice ensembles [5,6].

As the effective theory of QCD in the nonperturbative regime, chiral perturbation theory (ChPT) plays an important role. It allows one to determine the light-quark (u, d) mass dependence of low-energy hadronic observables in terms of low-energy constants (LECs) and perform model-independent extrapolations of LQCD results to the physical point. ChPT also allows one to account for finite lattice-volume and lattice-spacing corrections in a systematic way [7,8]. It has also proved helpful to deal with the contamination from excited states [5,6,9]. The interplay between ChPT and LQCD can also be used to determine poorly known LECs, which are difficult to access with experimental data. This is the case of d_{16} present in the $\mathcal{O}(p^3)$ part of the πN Lagrangian. Via a $4d_{16}M_\pi^2$ term, this LEC controls the slope of the light-quark mass dependence of g_A.[2] Therefore, its extraction from LQCD results at low pion masses is only natural. LEC d_{16} has been identified as one of the most significant sources of uncertainty in quark mass dependence of nuclear properties such as ground-state and binding energies through long-range nuclear forces [10–12].

Alternatively, LECs have been extracted from experimental information[3] on various processes such as pion photo- and electroproduction [13–16] but, predominantly, from pion-nucleon (πN) scattering [17–25]. Although d_{16} cannot be extracted from πN elastic scattering, it contributes significantly to inelastic, $\pi N \to \pi\pi N$, scattering.

---

[*]Fernando.Alvarado@ific.uv.es
[†]Luis.Alvarez@ific.uv.es
[1]After taking into account radiative corrections, a numerical value of $g_A = 1.2754(13)_{\text{exp}}(2)_{\text{RC}}$ has been recently extracted [1] from the PDG average $g_A/g_V = 1.2756(13)$ [2].

[2]Let us recall that in the isospin-symmetric limit $m_u = m_d \equiv \hat{m}$, $M_\pi^2 = 2B_0\hat{m} + \mathcal{O}(p^4)$, so that, as customary, we indistinctly refer to the $\hat{m}$ or M_π dependence.
[3]Throughout this article, LECs obtained from experimental data are called phenomenological or empirical to distinguish them from those extracted from LQCD simulations.

Indeed, in a combined fit to both elastic and inelastic πN scattering data, d_{16} has been recently extracted, albeit with a large uncertainty [26]. Baryon ChPT (BChPT) has been used to calculate the axial charge within the heavy-baryon [27–31] and relativistic [22,23,30,32–35] ChPT approaches both without and with the $\Delta(1232)$ as an explicit degree of freedom. In the relativistic framework, both infrared and extended-on-mass-shell (EOMS) regularization methods have been applied. Some of these studies also address the nucleon axial form factor at low four-momentum transfers squared [32–35]. The M_π dependence of g_A has been specifically investigated in Refs. [28–31,34,35].

Armed with relativistic baryon ChPT, we revisit this problem up to next-to-next-to-leading order (NNLO) in the perturbative expansion. The EOMS scheme ensures that not only power counting but also analytic properties of loop functions are properly preserved. After describing in Sec. II the details of the ChPT calculation and introducing the relevant terms of the effective Lagrangian, we show in Sec. III the M_π dependence of g_A predicted with the phenomenological LECs obtained in Ref. [26] from πN elastic and inelastic scattering. In order to obtain a better description of recent LQCD data, we have performed fits from which some of the LECs and, in particular, d_{16}, are determined. These are presented in Sec. IV. A meaningful representation of the flat trend exhibited by the LQCD results is only achieved with explicit $\Delta(1232)$. Differences between orders, which are considerable between NLO and NNLO, are used to provide a measure of the systematic error arising from the truncation of the perturbative series. These differences are the main source of uncertainty in the extracted d_{16} value.

II. THE NUCLEON AXIAL CHARGE IN RELATIVISTIC BChPT

In the isospin limit, the matrix element of the axial isovector current

$$A_\mu^a(x) = \bar{q}(x)\gamma_\mu\gamma_5\frac{\tau^a}{2}q(x), \tag{1}$$

with $q = (u, d)^T$ the quark-field doublet, taken between on-shell nucleon states of equal four-momenta p ($p^2 = m_N^2$), can be written as

$$\langle N(p)|A_\mu^a(0)|N(p)\rangle = \bar{u}(p)g_A\gamma_\mu\gamma_5\frac{\tau^a}{2}u(p). \tag{2}$$

The isovector character of the current is manifest given the presence of the Pauli isospin matrices τ^a.

We calculate the axial charge g_A employing relativistic BChPT with pions, nucleons, and Δ as degrees of freedom. We use the standard power counting [36], extended to diagrams with Δ baryons following small scale expansion

of Refs. [37,38]. In this power counting, the mass difference $\delta = m_N - m_\Delta$ is $\mathcal{O}(p)$.

A. Relevant terms of the effective Lagrangian

In this section, the terms in the effective Lagrangian, $\mathcal{L}_{\text{eff}}$, required for our calculation are presented. We need

$$\mathcal{L}_{\text{eff}} \supset \mathcal{L}_{\pi N}^{(1)} + \mathcal{L}_{\pi\Delta}^{(1)} + \mathcal{L}_{\pi N\Delta}^{(1)} + \mathcal{L}_{\pi N}^{(2)} + \mathcal{L}_{\pi N\Delta}^{(2)} + \mathcal{L}_{\pi\Delta}^{(2)} + \mathcal{L}_{\pi N}^{(3)}, \tag{3}$$

where superscripts indicate the chiral order, and subscripts show the present degrees of freedom. The terms in $\mathcal{L}_{\pi N}^{(1,3)}$, $\mathcal{L}_{\pi\Delta}^{(1)}$, and $\mathcal{L}_{\pi N\Delta}^{(1)}$ that are relevant for our study have been displayed in Ref. [34] using the same notation adopted here. In addition, $\mathcal{O}(p^2)$ contributions are entailed to give g_A at NNLO. Following the notation of Ref. [39], the required terms of the πN Lagrangian are

$$\mathcal{L}_{\pi N}^{(2)} \supset \bar{\Psi}\left(c_1\langle\chi_+\rangle - \frac{c_2}{8\overset{\circ}{m}^2}(\langle u_\mu u_\nu\rangle\{D^\mu, D^\nu\} + \text{H.c.})\right.$$
$$\left. + \frac{c_3}{2}\langle u_\mu u^\mu\rangle + \frac{ic_4}{4}[u_\mu, u_\nu]\sigma^{\mu\nu}\right)\Psi, \tag{4}$$

where Ψ is the isospin doublet of nucleon fields. Including only isovector axial external fields $a_\mu^a\tau^a/2 \equiv a_\mu$, we end up with

$$\begin{aligned} D_\mu &= \partial_\mu + \Gamma_\mu, \\ \Gamma_\mu &= \frac{1}{2}[u^\dagger(\partial_\mu - ia_\mu)u + u(\partial_\mu + ia_\mu)u^\dagger], \\ u_\mu &= i[u^\dagger(\partial_\mu - ia_\mu)u - u(\partial_\mu + ia_\mu)u^\dagger]; \end{aligned} \tag{5}$$

$\chi^+ = u^\dagger\chi u^\dagger + u\chi^\dagger u$, with $\chi = \text{diag}(M_\pi^2, M_\pi^2)$, and $\langle\ldots\rangle$ denotes a trace over isospin.

In $\mathcal{L}_{\pi N\Delta}^{(2)}$, after redundant terms are eliminated from Eq. (67) of Ref. [40] (see also Sec. 3.1 of Ref. [41] and the Appendix of Ref. [42]), only the following monomials,

$$\mathcal{L}_{\pi N\Delta}^{(2)} \supset \bar{\Psi}_\alpha^k\xi_{ki}^{\frac{3}{2}}\left\{\frac{b_4}{2}\omega_\alpha^i\omega_\beta^j\gamma^\beta\gamma_5\tau^j + \frac{b_5}{2}\omega_\alpha^j\omega_\beta^i\gamma^\beta\gamma_5\tau^j\right\}\Psi$$
$$+ \text{H.c.}, \tag{6}$$

contribute to the nucleon axial charge. Here, Ψ_μ denotes the Rarita-Schwinger field of the Δ resonance. States $\{\xi_{ij}^{\frac{3}{2}}\Psi_\mu^j\}_{i=1-3}$, where $\xi_{ij}^{\frac{3}{2}} = \delta_{ij} - \tau_i\tau_j/3$ are isospin-3/2 projectors, are also isospin doublets, whose explicit expressions in terms of the physical Δ states are derived, for example, in Appendix A of Ref. [43]. The isovector projection of u^μ is represented by $\omega^{\mu,i} = \frac{1}{2}\langle\tau^i u^\mu\rangle$ (see, for instance, Ref. [40]). Finally, also at $\mathcal{O}(p^2)$ [40,44],

$$\mathcal{L}_{\pi\Delta}^{(2)} \supset \bar{\Psi}_\mu^i\xi_{ij}^{\frac{3}{2}}\{a_1\langle\chi_+\rangle\delta^{jk}g_{\mu\nu}\}\xi_{kl}^{\frac{3}{2}}\Psi^{l\nu} \tag{7}$$
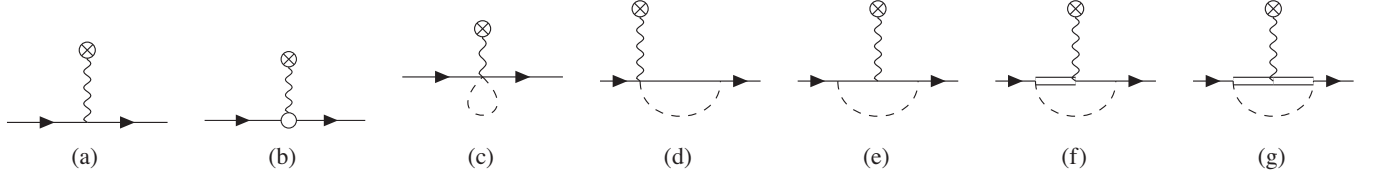
FIG. 1.   Diagrams at orders $\mathcal{O}(p)$, (a), and $\mathcal{O}(p^3)$, (b)–(g), contributing to the nucleon axial charge. Dashed, solid single, and double lines denote pions, nucleons, and Δ resonances, respectively; wiggly lines stand for external axial fields. The open circle represents an $\mathcal{O}(p^3)$ vertex, while the rest of the vertices are $\mathcal{O}(p)$. Permutations of diagrams (d) and (f) have been omitted in the figure.
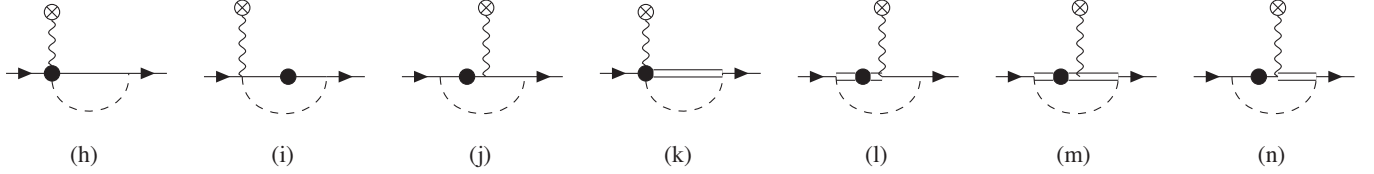

FIG. 2. $\mathcal{O}(p^4)$ diagrams contributing to the nucleon axial charge. Line styles are the same as in Fig. 1. Filled circles denote $\mathcal{O}(p^2)$ vertices. Permutations of all these diagrams are taken into account but not explicitly represented.

introduces an M_π-dependent correction to the Δ mass, in the same way as the term proportional to c_1 does for the nucleon mass.

B. Perturbative calculation

The set of Feynman diagrams that contribute to the axial form factor and, in particular, to g_A are displayed in Figs. 1 and 2. The LECs that each of these diagrams brings about are listed in Table I. At $\mathcal{O}(p^4)$, there are contributions from $\mathcal{O}(p^2)$ vertices but also baryon (N, Δ) mass insertions. The later are calculated perturbatively; i.e., we evaluate directly diagrams (i), (j), and (l)–(n) of Fig. 2, avoiding Dyson resummations to all orders in the propagators. Alternative choices have been considered in Refs. [33,35].

Although not diagrammatically represented, nucleon wave-function renormalization is taken into account in the standard way. To the order of our calculation, only the $\mathcal{O}(p)$ diagram (a), giving just the axial charge in the chiral limit $\overset{\circ}{g}_A$, should be multiplied by the wave-function renormalization constant Z_N, calculated from the $\mathcal{O}(p^4)$ nucleon self-energy,

$$Z_N \approx 1 + \left.\frac{\partial \Sigma_N^{(4)}}{\partial \not{p}}\right|_{\not{p}=m_N}. \qquad (8)$$

Additional $\mathcal{O}(p^3)$ and $\mathcal{O}(p^4)$ contributions to g_A are generated in this way. The LECs that enter in them are also listed in Table I.

In order to absorb the ultraviolet divergencies generated by loops, we perform dimensional renormalization in the $\widetilde{\text{MS}}$ scheme [45], at the scale $\mu = \overset{\circ}{m}$, where $\overset{\circ}{m}$ denotes the nucleon mass in the chiral limit. An additional

renormalization is then performed to account for the power-counting breaking caused by the presence of baryon masses which do not vanish in the chiral limit. Among the available schemes, we employ EOMS renormalization [45] which consists of the absorption of the power-counting breaking (PCB) terms in a redefinition of the LECs. In this way, power counting is restored without altering the analytic properties of the loops and preserving covariance. Note that, as in earlier studies [24,34], PCB terms are identified and subtracted in an expansion in powers or M_π but not in δ. The EOMS renormalization shifts for the LECs are lengthy, so we have included them in the Supplementary Material [46].

TABLE I.   LECs introduced by Feynman diagrams in Figs. 1 and 2 and by wave-function renormalization (wfr).

Diagrams	$\mathcal{O}(p)$	$\mathcal{O}(p^2)$	$\mathcal{O}(p^3)$
(a), (c), (d)	$\overset{\circ}{g}_A$	$\cdots$	$\cdots$
(b)	$\cdots$	$\cdots$	d_{16}
(e)	$\overset{\circ}{g}_A$	$\cdots$	$\cdots$
(f)	$\overset{\circ}{g}_A, h_A$	$\cdots$	$\cdots$
(g)	g_1, h_A	$\cdots$	$\cdots$
(h)	$\overset{\circ}{g}_A$	c_{2-4}	$\cdots$
(i)	$\overset{\circ}{g}_A$	c_1	$\cdots$
(j)	$\overset{\circ}{g}_A$	c_1	$\cdots$
(k)	h_A	$b_{4,5}$	$\cdots$
(l)	$\overset{\circ}{g}_A, h_A$	a_1	$\cdots$
(m)	g_1, h_A	a_1	$\cdots$
(n)	$\overset{\circ}{g}_A, h_A$	c_1	$\cdots$
wfr	$\overset{\circ}{g}_A, h_A$	c_1, a_1	$\cdots$

In the way outlined above, we obtain the axial charge within the EOMS renormalization scheme up to $\mathcal{O}(p^4)$ with explicit Δ. Our result has the following structure, with superindices indicating the chiral order,

$$
\begin{aligned}
g_A = {} & \mathring{g}_A + 4d_{16}M_\pi^2 + g_{A(\text{loop})}^{(3)\cancel{\Delta}}(\mathring{g}_A; M_\pi) \\
& + g_{A(\text{loop})}^{(3)\Delta}(\mathring{g}_A, h_A, g_1; M_\pi) \\
& + g_{A(\text{loop})}^{(4)\cancel{\Delta}}(\mathring{g}_A, c_1, c_2, c_3, c_4; M_\pi) \\
& + g_{A(\text{loop})}^{(4)\Delta}(\mathring{g}_A, h_A, g_1, c_1, a_1, b_4, b_5; M_\pi) + \mathcal{O}(p^5).
\end{aligned} \quad (9)
$$

The structures arising from the loops are preserved at the price of keeping higher order terms. The $\mathcal{O}(p^3)$ part of g_A is given in Eq. (A4) of Ref. [34]. In Appendix B, we provide the $\mathcal{O}(p^4)$ contribution from wave-function renormalization. The length of the rest of the $\mathcal{O}(p^4)$ expression, which depends on several LECs, discourages us from giving it explicitly but is available in a Mathematica notebook as supplementary material [46]. We nonetheless identify that at $\mathcal{O}(p^4)$, i.e., at $\mathcal{O}(M_\pi^3)$ for g_A, c_3 and c_4 enter in the following combination, $\tilde{c}_4 = c_4 - c_3/2$, while c_2 enters only at $\mathcal{O}(p^5)$ [$\mathcal{O}(M_\pi^4)$ in g_A]. Although the rather involved contribution of diagram (k) does not, *a priori*, show the factorization of any mixture of b_4 and b_5 LECs, after expanding in M_π, one finds that the combination which actually enters at $\mathcal{O}(p^4)$ is $\tilde{b}_4 = b_4 + (12/13)b_5$. At $\mathcal{O}(p^3)$, we reproduce the results of Eq. (A4) of Ref. [34]. At $\mathcal{O}(p^4)$, we agree with the $\cancel{\Delta}$ EOMS expressions given in Refs. [22,33] except for the different treatment of nucleon mass insertions, which in our case do not include resummations. As a result, $c_1 M_\pi^2$ factors appear only linearly in our calculation but not at all orders. Furthermore, a PCB term proportional to c_4 present in Ref. [22] after the EOMS renormalization is absent in our final result.

III. LIGHT-QUARK MASS DEPENDENCE OF THE AXIAL COUPLING FROM PHENOMENOLOGICAL INPUT

Once the framework and the chiral order are established, the M_π dependence of g_A is ultimately determined by the LEC values. In Ref. [26], elastic πN and inelastic $\pi N \to \pi\pi N$ scattering has been studied up to $\mathcal{O}(p^4)$ in covariant ChPT using a modified version of the EOMS approach [25]. The LECs that enter $g_A(M_\pi)$ at $\mathcal{O}(p^4)$ in the Δ-less model were extracted, including d_{16}, owing to the inclusion of low energy total and double differential $\pi N \to \pi\pi N$ cross section data in the combined analysis. To make a prediction of $g_A(M_\pi)$ based on this phenomenological input, we should transform the LECs from the modified EOMS of Refs. [25,26] to the conventional one adopted here. To the order we are working at, this transformation,

TABLE II. LECs used to obtain the $g_A(M_\pi)$ dependence in the $\cancel{\Delta}$ case.

	$\mathcal{O}(p^3)$	$\mathcal{O}(p^4)$
$\mathring{g}_A$	1.251 ± 0.051	1.089 ± 0.030
d_{16} (GeV^{-2})	-2.2 ± 1.1	-1.86 ± 0.80
c_1 (GeV^{-1})	$\cdots$	-0.89 ± 0.06
c_2 (GeV^{-1})	$\cdots$	3.38 ± 0.15
c_3 (GeV^{-1})	$\cdots$	-4.59 ± 0.09
c_4 (GeV^{-1})	$\cdots$	3.31 ± 0.13

whose details are disclosed in Appendix A, affects the numerical value of d_{16} but not of c_{1-4}. The axial coupling in the chiral limit, $\mathring{g}_A$, which is not extracted in Refs. [25,26], is determined as

$$
\begin{aligned}
g_A(M_\pi = M_{\pi(\text{phys})}, \mathring{g}_A, d_{16}, c_i) &= g_{A(\text{phys})} \\
&= 1.2754(13)_{\text{exp}}(2)_{\text{RC}} \quad (10)
\end{aligned}
$$

from the experimental value, precisely known from β decay [1]. Up to higher orders for g_A, the remaining parameters, i.e., the pion decay constant and the nucleon mass in the chiral limit, have been fixed to $F_\pi \simeq F_{\pi(\text{phys})} = 92.2$ MeV and $\mathring{m} \simeq m_{\text{N(phys)}} + 4c_1 M_{\pi(\text{phys})}^2$, with $M_{\pi(\text{phys})} = 135$ MeV and $m_{\text{N(phys)}} = 939$ MeV, respectively. The numerical values for d_{16}, c_{1-4} as well as $\mathring{g}_A$ and their uncertainties are summarized in Table II.

The resulting $g_A(M_\pi)$ at $\mathcal{O}(p^3)$ and $\mathcal{O}(p^4)$ are displayed in Fig. 3 together with a subset of recent LQCD
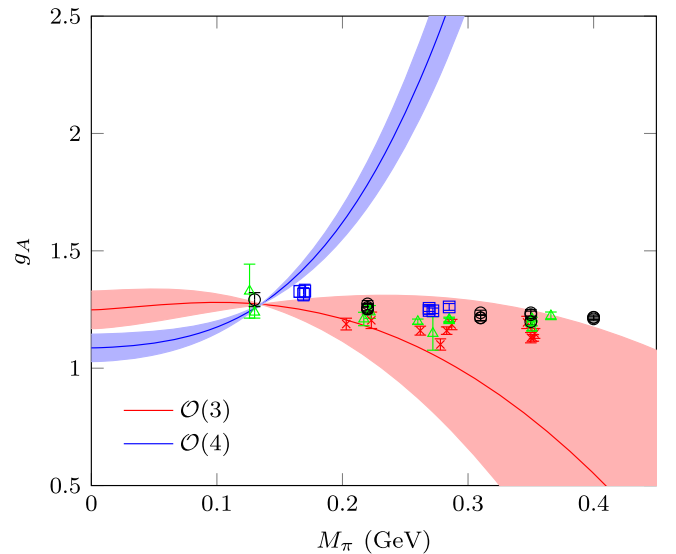

FIG. 3. Pion-mass dependence of g_A at $\mathcal{O}(p^3)$ (red) and $\mathcal{O}(p^4)$ (blue) using phenomenological input from Ref. [26] and 1σ error bands. The LQCD data points are from CalLat 18 [47] (black circles), Mainz 19 [48] (red crosses), RQCD 19 [9] (green triangles), and NME 21 [49] (blue squares).

determinations.[4] The curves are accompanied by 1σ statistical error bands arising from the uncertainties in the LECs of Table II assuming they are Gaussian distributed. Unaccounted correlations are negligible because the uncertainty is strongly dominated by the d_{16} error. The $\mathcal{O}(p^3)$ result shows agreement with the lattice determinations, albeit with increasing tension as M_π grows and a curvature in the central value that is absent in the data. On the other hand, it is immediately apparent that the $\mathcal{O}(p^4)$ prediction not only does not improve the $\mathcal{O}(p^3)$ but plainly fails to describe the M_π dependence of LQCD data. We have checked that alternative c_{1-4} determinations from earlier πN analyses using EOMS [22,24] do not mitigate the steep rise of $g_A(M_\pi)$ at $\mathcal{O}(p^4)$. Therefore, the inability to reconcile the light-quark mass dependence of $\overset{\circ}{g}_A$ at $\mathcal{O}(p^4)$ with phenomenology, earlier observed in nonrelativistic heavy-baryon ChPT [29,30], is also a feature of the relativistic version of the theory.

The problem with the $\mathcal{O}(p^4)$ result might be caused by an accidental slow convergence of g_A in BChPT. Instead, one could argue that additional degrees of freedom such as the Δ [30] or even the Roper $N(1440)$ resonance might solve the issue. In Ref. [26], a version of the theory incorporating the Δ pole is also considered. However, in order to predict $g_A(M_\pi)$ up to $\mathcal{O}(p^4)$ with explicit Δ, additional LECs absent in that study are needed. For this reason, we do not tackle the role of the Δ in the $g_A(M_\pi)$ dependence from purely empirical input but postpone it to the next Sec. IV where our fits to recent LQCD data are reported.

IV. ANALYSIS OF LQCD RESULTS AND LEC DETERMINATION

A. Data set and fit strategy

The axial charge has been historically underpredicted in the lattice (see, for instance, Fig. 2 of Ref. [50]), but, as a result of conceptual and technical improvements, the majority of LQCD results nowadays agree with the experimental value at the level of a few percent [4]. Most significantly, the analysis of excited-state contamination has notably evolved in last years. Therefore, we only include in our data set results from studies with an improved treatment of these effects. We take into account renormalized $\{g_A^i\}$ data at different $\{M_\pi^i, a_i\}$ values, where a stands for the lattice spacing, from[5] CalLat 18 [47], Mainz 19 [48], RQCD 19 [9],[6] and NME 21 [49].[7] Our

---

[4]The selection criteria for the LQCD data are discussed in Sec. IV A.
[5]The names are borrowed from the FLAG Review 2021 [4].
[6]We only consider the simulations with $m_s \sim m_{s(\mathrm{phys})}$, the ones suitable for an SU(2) ChPT analysis.
[7]We take the results from the fit strategy labeled as $\{4^{N\pi}, 3^*\}$, used to control excited-state contamination, averaging over the two renormarization methods Z_1 and Z_2.

analysis treats $2 + 1 + 1$ (CalLat 18) and $2 + 1$ (Mainz 19, RQCD 19, NME 21) ensembles on the same footing, assuming that the c-quark sea content plays a negligible role. We disregard LQCD determinations of g_A coming from q^2, finite volume, a, or M_π extrapolations. Since we do not correct the finite volume effects, we consider only large volumes, satisfying $M_\pi L \geq 3.5$, so that the neglected extrapolation is small and can be absorbed in the errors.

In order to gauge the ability of BChPT at $\mathcal{O}(p^3)$ and $\mathcal{O}(p^4)$ to describe the M_π dependence of g_A, and to extract $\overset{\circ}{g}_A$ and d_{16} LECs, we perform fits to the LQCD data set defined above. With this aim, we define the following χ^2,

$$\chi^2 = \sum_i \frac{(g_A(M_\pi^i, a_i) - g_A^i)^2}{(\Delta g_A^i)^2} + \chi^2_{\mathrm{prior}}. \qquad (11)$$

In addition to $g_A(M_\pi)$ from BChPT, our theoretical parametrization incorporates lattice discretization corrections as

$$g_A(M_\pi^i, a_i) = g_A(M_\pi^i) + x_j a_i^{n_j}. \qquad (12)$$

Free parameters x_j, with $j = 1, 2, 3, 4$ when lattice data point $i \in \{\mathrm{CalLat\,18, Mainz\,19, RQCD\,19, NME\,21}\}$, respectively, control the leading a dependence of the LQCD data, which is action specific, $n_{1,4} = 1$, while $n_{2,3} = 2$. These discretization corrections are small and do not substantially change the extracted LECs but result in an appreciable reduction of the fits' $\chi^2/\mathrm{d.o.f.}$

Some of the LECs upon which $g_A(M_\pi)$ depends are well determined in other studies and are kept fixed, while others are treated as free parameters together with $\overset{\circ}{g}_A$ and d_{16}. To improve our description of the LQCD data and reduce correlations [51], for free LECs, we assume naturalness $\Lambda^{n-1} c_n \sim 1$, encoded in Gaussian priors,

$$\chi^2_{\mathrm{prior}} = \sum_{\mathrm{free\,LECs}} \left(\frac{\Lambda^{n-1} c_n}{5}\right)^2. \qquad (13)$$

Here, c_n generically denotes a LEC of chiral order $\mathcal{O}(p^n)$; the breakdown scale is set to $\Lambda = 1\text{ GeV} \sim 4\pi F_\pi$ [52,53]. We anticipate that a prior for $\overset{\circ}{g}_A$ is superfluous, since its value is always driven to a natural one by low M_π g_A^i LQCD data.

The large relative contribution of $\mathcal{O}(p^4)$ terms discussed in the previous section and illustrated by Fig. 3 is a clear indication that the theoretical error associated with truncation of the perturbative expansion should be taken into account. We follow the method proposed in Ref. [54]. Let X be an observable with a chiral perturbative expansion,

$$X = X^{(0)} + \sum_{m=1}^{\infty} \Delta X^{(m)}; \qquad (14)$$

$\Delta X^{(m)} = X^{(m)} - X^{(m-1)}$ encompasses all the monomials that start at order m. If X is calculated up to order n, $X \approx X^{(n)}$, assuming that the truncation error is dominated by order $n + 1$, its contribution $\Delta X^{(n+1)}$ can be estimated in a conservative way as [25,54]

$$|\Delta X^{(n+1)}| = \max\left\{Q^{n+1}|X^{(0)}|, Q^n|\Delta X^{(1)}|, \ldots, Q|\Delta X^{(n)}|\right\},$$ (15)

where Q denotes the expansion variable.

For g_A, $Q = M_\pi/\Lambda$. Recalling that in this case $\mathcal{O}(p^5) = \mathcal{O}(M_\pi^4)$, for our $\mathcal{O}(p^4)$ calculation, Eq. (15) gives

$$\Delta g_{A\chi}^{(5)} = \max\left\{\left(\frac{M_\pi}{\Lambda}\right)^4|\mathring{g}_A|, \left(\frac{M_\pi}{\Lambda}\right)^2|\Delta g_A^{(3)}|, \frac{M_\pi}{\Lambda}|\Delta g_A^{(4)}|\right\}$$
$$\sim Q^4 = \mathcal{O}(p^5).$$ (16)

Connecting to Eq. (9), $\Delta g_A^{(3)} = 4d_{16}M_\pi^2 + g_{A(\text{loop})}^{(3)}$ and $\Delta g_A^{(4)} = g_{A(\text{loop})}^{(4)}$. Based on the results in Sec. III, it is easy to foresee that at larger M_π, $\Delta g_{A\chi}^{(5)}$ will be determined by the last term in Eq. (16). In our $\mathcal{O}(p^3)$ fits, we do not assume any prior knowledge about $\mathcal{O}(p^4)$, and therefore, the truncation error is given by

$$\Delta g_{A\chi}^{(4)} = \max\left\{\left(\frac{M_\pi}{\Lambda}\right)^3|\mathring{g}_A|, \frac{M_\pi}{\Lambda}|\Delta g_A^{(3)}|\right\} \sim Q^3$$
$$= \mathcal{O}(p^4).$$ (17)

In our χ^2, Eq. (11), this theoretical error is added in quadrature to the one of LQCD points,

$$(\Delta g_A^i)^2 = (\Delta g_{\text{ALQCD}}^i)^2 + (\Delta g_{A\chi}(M_\pi^i))^2.$$ (18)

This recipe assigns larger uncertainties to points at high M_π, where the convergence of the chiral expansion is poorer, therefore reducing their impact on the fit. We should also mention that, as discussed in Refs. [25,54,55], although this theoretical error estimate does not have a clear statistical interpretation, results are similar to those obtained in a preferable but beyond the scope of the present study Bayesian approach [51].

Fits are carried out iteratively until convergence is achieved. The first minimization is performed without theoretical errors, which are subsequently evaluated using the LECs determined in the previous step. The lattice discretization parameters x_j are fixed in the first iteration because evolving them results in overfitting. With the described procedure, LQCD and truncation errors are not independent, and it is not obvious how to combine them in the error for a given observable. Consequently, following Ref. [25], we plot them separately in the error bands for $g_A(M_\pi)$. Furthermore, as a quantitative measure of the

agreement of our best-fit curve with the LQCD data, we also provide the χ_0^2 value, defined as

$$\chi_0^2 = \sum_i \frac{(g_A(M_\pi^i, a_i) - g_A^i)^2}{(\Delta g_{\text{ALQCD}}^i)^2}.$$ (19)

Finally, we have tested the convergence range of our calculation by varying the maximum M_π of the lattice data included in the fits in the range of $M_{\pi\text{cut}} \in [200, 402]$ MeV. A plateau in the χ^2 and the fitted LECs is found toward the end of the interval. In consequence, we report results including all points in the chosen data sets up to $M_\pi = 402$ MeV.[8] As discussed in Sec. IV C 2, the theoretical error becomes larger at higher M_π where the convergence is poorer, and therefore, the corresponding LQCD points weigh less in the fits.

B. $\cancel{\Delta}$ case

1. $\mathcal{O}(p^3)$

At $\mathcal{O}(p^3)$, the only free parameters (besides the x_j governing the a dependence) are $\mathring{g}_A$ and d_{16} LECs. The results of the fit are shown in the upper left panel of Fig. 4 and the first column of Table III. At the first sight, this model describes LQCD data well, with a good $\chi^2/\text{d.o.f.}$, relatively small errors, and natural $\mathring{g}_A$ and d_{16}. As apparent from the comparison of the first columns of Tables II and III, the d_{16} value is slightly above the phenomenological one extracted in Ref. [26] and with a much smaller error. Instead, $\mathring{g}_A$ is in tension with the value obtained from experimental input, Eq. (10). As a consequence, $g_A(M_{\pi(\text{phys})}) = 1.205 \pm 0.010$, well below the experimental result. However, an inspection of the results for the $\mathcal{O}(p^4)$ model described below reveals a large contribution from the $\mathcal{O}(p^4)$ terms at $M_\pi \gtrsim 200$ MeV, in line with the findings of Sec. III. The fact that these terms are considerably larger than the error band of the $\mathcal{O}(p^3)$ result implies that, in this case, the theoretical error estimated from $\mathcal{O}(p^1)$ and $\mathcal{O}(p^3)$ terms falls short in accounting for the $\mathcal{O}(p^4)$ contribution. The agreement of $g_A(M_\pi)$ at $\mathcal{O}(p^3)$ with LQCD points appears then as misleadingly good, while the uncertainties in the LEC values can be regarded as underestimated. In other words, to be realistic, an $\mathcal{O}(p^3)$ analysis should be limited to small $M_\pi < 200$ MeV, which would be unfeasible with the small amount of presently available LQCD data in this region.

2. $\mathcal{O}(p^4)$

In the $\mathcal{O}(p^4)$ $\cancel{\Delta}$ model, one has the additional contribution of NLO LECs c_{1-4}. They were initially allowed to

---

[8]This upper limit allows one to include available points close but above $M_\pi = 400$ MeV.
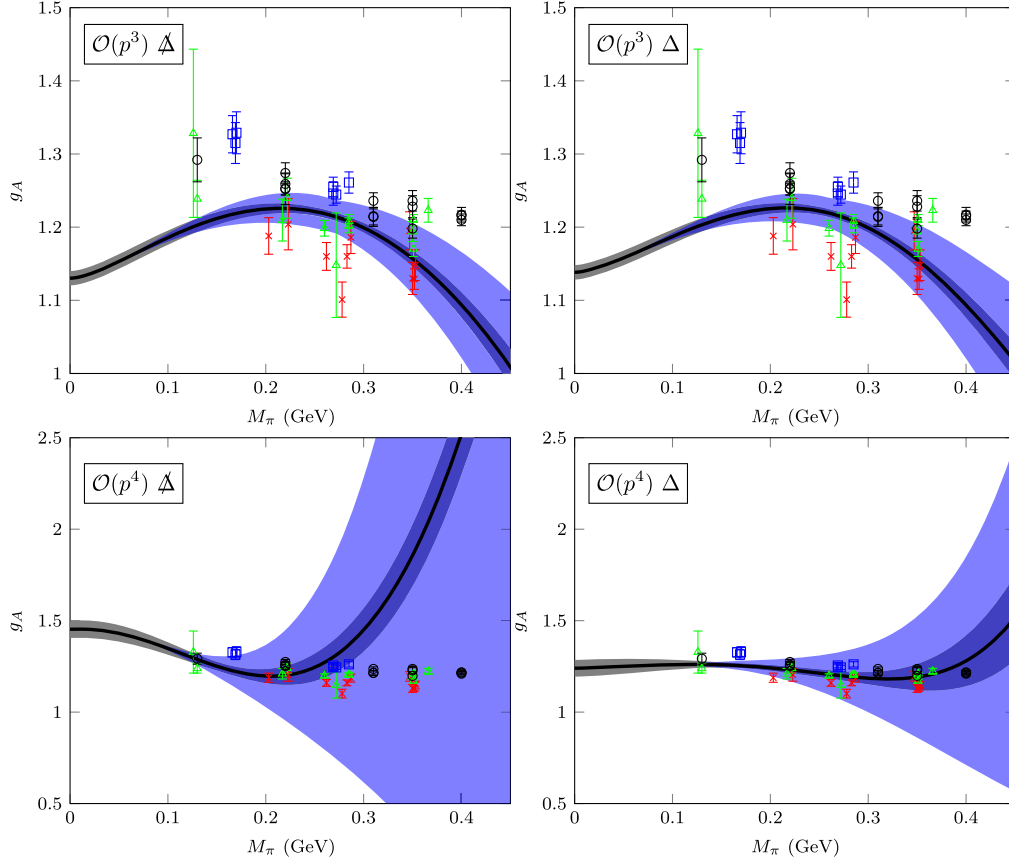
FIG. 4. Pion-mass dependence of g_A obtained by fitting LQCD results with $\mathcal{O}(p^3)$ and $\mathcal{O}(p^4)$ relativistic BChPT without and with $\Delta(1232)$ as explicit degree of freedom. Gray (dark) bands correspond to errors determined by propagating LEC uncertainties. Blue bands represent the estimated theoretical uncertainties $\Delta g_{A\chi}^{(4,5)}$. The LQCD points from CalLat 18 [47] (black circles), Mainz 19 [48] (red crosses), RQCD 19 [9] (green triangles), and NME 21 [49] (blue squares) are shown at their finite a values, i.e., without (small) discretization corrections.

evolve in the fits under the constrains set by their empirical determination [26] (second column of Table II) implemented as Gaussian priors. However, as these LECs are quite well determined, this procedure yields substantially the figures favored by the priors. Therefore, we report here the results of a simpler fit with c_{1-4} held fixed to their central phenomenological values (second column of Table III).

In any case, as apparent from the lower left panel of Fig. 4, the $\mathcal{O}(p^4)$ $\not{\Delta}$ model fails to describe the light-quark mass dependence of g_A.[9] The small χ^2 is merely a consequence of the large theoretical error, which reduces the impact of high M_π points on the fit. Nevertheless, the poor agreement is reflected in the magnitude of χ_0^2 and also in the quite unnatural d_{16} in spite of its prior. This large (in absolute value) d_{16} is inconsistent with its phenomenological value and nonetheless unable to correct the M_π dependence at $M_\pi \gtrsim 300$ MeV, which is largely dominated

by the $\mathcal{O}(p^4)$ terms and, therefore, very similar to the one displayed in Fig. 3.

The fact that the very wide theoretical error band encompasses the lattice points reflects that the disagreement would be removed by a (large) contribution of $\mathcal{O}(p^5)$ counterbalancing the $\mathcal{O}(p^4)$ ones. Actually, within heavy-baryon ChPT, it has been shown [29] that the curve can be *bent down* by additional contributions of orders $\mathcal{O}(p^{5,6})$ with LECs of natural size (see also Fig. 1 of Ref. [11]). Here, we take a different avenue and introduce the $\Delta(1232)$ explicitly as advocated in Ref. [30] based on the Adler-Weisberger sum rule [56,57] and a heavy-baryon ChPT calculation for g_A.

C. Δ case

With the $\Delta(1232)$ as explicit degree of freedom (d.o.f.), new contributions with additional LECs arise. We fix the $\mathcal{L}_{\pi N\Delta}^{(1)}$ coupling h_A to its large-N_c value $h_A = 1.35$ [26], which is close to its empirical value [24]. For the $\mathcal{L}_{\pi\Delta}^{(1)}$ coupling g_1, whose impact on g_A is small, the large-N_c limit

---

[9]Lattice-spacing corrections were neglected in this fit once they become unnaturally large (and uncertain) leading to overfitting.

TABLE III. LEC values, both fixed and fitted to LQCD data, in the four different models under study. The χ^2/d.o.f. for each fit is given at the bottom; χ_0^2, defined in Eq. (19), does not include theoretical errors or naturalness priors.

	$\mathcal{O}(p^3)\ \slashed{\Delta}$	$\mathcal{O}(p^4)\ \slashed{\Delta}$	$\mathcal{O}(p^3)\ \Delta$	$\mathcal{O}(p^4)\ \Delta$
$\mathring{g}_A$ (free)	1.1302 ± 0.0098	1.453 ± 0.048	1.1383 ± 0.0099	1.240 ± 0.046
d_{16} (GeV^{-2}) (free)	-0.925 ± 0.055	-9.77 ± 0.87	1.224 ± 0.040	-0.88 ± 0.88
h_A	$\cdots$	$\cdots$	1.35	1.35
g_1	$\cdots$	$\cdots$	-2.29	-2.29
c_1 (GeV^{-1})	$\cdots$	-0.89 ± 0.06	$\cdots$	-1.15 ± 0.05
c_2 (GeV^{-1})	$\cdots$	3.38 ± 0.15	$\cdots$	1.57 ± 0.10
c_3 (GeV^{-1})	$\cdots$	-4.59 ± 0.09	$\cdots$	-2.54 ± 0.05
c_4 (GeV^{-1})	$\cdots$	3.31 ± 0.13	$\cdots$	2.61 ± 0.10
a_1 (GeV^{-1})	$\cdots$	$\cdots$	$\cdots$	0.90
$\tilde{b}_4$ (GeV^{-2}) (free)	$\cdots$	$\cdots$	$\cdots$	-12.3 ± 1.0
x_1 (fm^{-1})	0.39 ± 0.68	$\cdots$	0.38 ± 0.07	0.21 ± 0.07
x_2 (fm^{-2})	-8.10 ± 1.80	$\cdots$	-8.17 ± 1.80	-7.27 ± 1.80
x_3 (fm^{-2})	2.25 ± 1.83	$\cdots$	2.17 ± 1.83	3.28 ± 1.84
x_4 (fm^{-1})	0.61 ± 0.11	$\cdots$	0.60 ± 0.11	0.51 ± 0.11
$\mathring{m}$ (GeV)	0.874	0.874	0.855	0.855
$\mathring{m}_\Delta$ (GeV)	$\cdots$	$\cdots$	1.166	1.166
χ^2/d.o.f.	$36.06/(43-6) = 0.98$	$13.31/(43-2) = 0.33$	$37.60/(43-6) = 1.02$	$11.14/(43-7) = 0.31$
χ_0^2/d.o.f.	$424.87/(43-6) = 11.48$	$122820.67/(43-2) = 2995.63$	$439.19/(43-6) = 11.87$	$501.62/(43-7) = 13.93$

yields $|g_1| = 2.29$ [24,26]. We are unable to discern its sign in our fits to g_A LQCD data and opt for $g_1 = -2.29$, preferred both by πN elastic scattering [24] and our own studies of the nucleon axial form factor at low q^2 to be reported elsewhere. Finally, in analogy to the nucleon case, $\mathring{m}_\Delta \simeq m_{\Delta(\text{phys})} - 4a_1 M_{(\text{phys})}^2$ with $m_{\Delta(\text{phys})} = 1232$ MeV and $a_1 = 0.90$ GeV^{-1} from the LQCD M_π dependence of the Δ mass [58].

1. $\mathcal{O}(p^3)$

With this model, the result of the fit for $g_A(M_\pi)$ closely resembles the $\mathcal{O}(p^3)\ \slashed{\Delta}$ one as can be seen in the comparison of the upper panels of Fig. 3. However, the value of d_{16} changes considerably, including its sign, with respect to the $\mathcal{O}(p^3)\ \slashed{\Delta}$ one. The same feature was obtained when this LEC was extracted from LQCD results for the axial form factor at low q^2 with $\mathcal{O}(p^3)$ relativistic BChPT [34]. The $\mathcal{O}(p^4)$ fit described in the next section produces $\mathcal{O}(p^4)$ terms larger than the theoretical error estimated from $\mathcal{O}(p^1)$ and $\mathcal{O}(p^3)$ ones (although to a lesser extent than in the $\slashed{\Delta}$ case) making the extension to $\mathcal{O}(p^4)$ desirable for a more realistic determination of LECs and their uncertainties.

2. $\mathcal{O}(p^4)$

In the fit of the $\mathcal{O}(p^4)$ model with explicit Δ, we fix the c_{1-4} LECs to the values extracted from the πN scattering [25] (see the last column of Table III). They take the Δ pole into account and are in good agreement with the joint $\pi N + \pi\pi N$ fit from Ref. [26]. In addition to $\mathring{g}_A$ and d_{16}, we now have

$\mathcal{O}(p^2)b_4$ and b_5 LECs as free parameters. As mentioned in Sec. II B, these LECs appear at $\mathcal{O}(p^4)$ [more precisely, at $\mathcal{O}(M_\pi^4/\delta)$] in the combination $\tilde{b}_4 = b_4 + (12/13)b_5$. Therefore, we keep only $\tilde{b}_4$ as a free parameter of the fit and neglect remaining higher order monomials proportional to b_5.

The result of the fit, depicted in the lower right panel of Fig. 4, satisfactorily describes the trend of $g_A(M_\pi)$ as predicted by LQCD up to relatively large M_π. The theoretical error is large and rapidly increasing with M_π due to the large contribution of $\mathcal{O}(p^4)$ terms. Nevertheless, the description of LQCD data and convergence are notably improved with respect to the $\mathcal{O}(p^4)\ \slashed{\Delta}$ model.

The extracted LECs are given in Table III. The $\tilde{b}_4$ value might seem unnatural, but one should keep in mind that it is a combination of LECs. As shown in Table IV, the correlations among LECs are sizable; they are an indication of degeneracy among the parameters that could be partially lifted by adding a new dimension to the fit (i.e., studying the axial form factor at finite q^2). The d_{16} value obtained from this model, $d_{16} = -0.88 \pm 0.88$ GeV^{-2}, is in good

TABLE IV. Correlation matrix for the fit with the $\mathcal{O}(p^4)\ \Delta$ model.

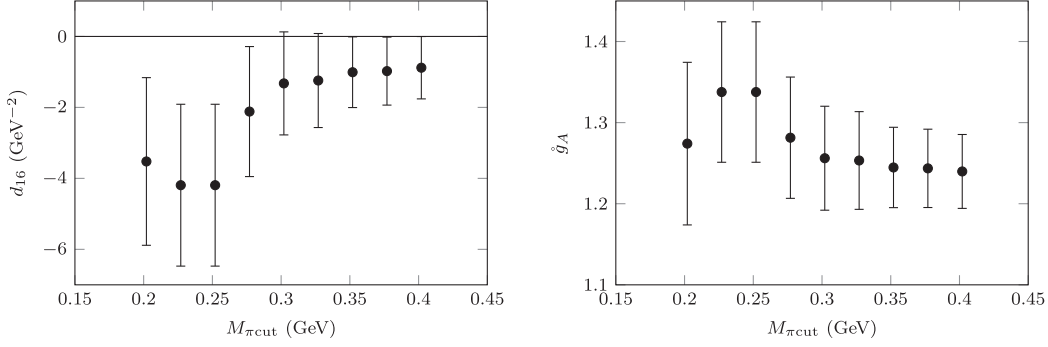|	$\mathring{g}_A$	d_{16}	$\tilde{b}_4$
$\mathring{g}_A$	1	-0.97	0.79
d_{16}		1	-0.92
$\tilde{b}_4$			1

FIG. 5.   Results of the fits for the $\mathcal{O}(p^4)$ model with explicit Δ as a function of the maximum $M_{\pi\mathrm{cut}}$.

agreement with the determination from inelastic $\pi N \to \pi\pi N$ with explicit Δ pole [26] which, translated to standard EOMS, is $d_{16(\mathrm{pheno})} = -1.0 \pm 1.0$ GeV^{-2}. Although, as argued in the Introduction, the M_π dependence of g_A is in principle better suited to extract d_{16} than the available experimental $\pi N \to \pi\pi N$ data, the convergence issues of the former lead to large errors, comparable to those of the phenomenological result. The $\mathring{g}_A$ value is higher than in the $\mathcal{O}(p^3)$ fits and with a larger error. Furthermore, at the physical point, $g_A(M_{\pi(\mathrm{phys})}) = 1.260 \pm 0.012$ is now close to the experimental value although with a much larger uncertainty.

The stability of the results for $\mathring{g}_A$ and d_{16} as a function of the maximum M_π considered, $M_{\pi\mathrm{cut}}$, is shown in Fig. 5. One can see that for both quantities the numerical values and their errors stabilize for $M_\pi \gtrsim 300$ MeV.

Owing to the consideration of theoretical errors, the analysis could be extended to a broader range of M_π because points at higher M_π, where the convergence is worse, have a larger combined uncertainty, Eq. (18), and contribute less to the fit.

V. CONCLUSIONS AND OUTLOOK

We have investigated the pion-mass dependence of the nucleon axial coupling up to $\mathcal{O}(p^4) \equiv \mathcal{O}(M_\pi^3)$ (NNLO) in relativistic BChPT with EOMS renormalization. We have shown that, at this order and without including $\Delta(1232)$ explicitly, the pion-mass dependence of g_A obtained using LECs extracted from phenomenological analyses of pion-nucleon elastic and inelastic ($\pi N \to \pi\pi N$) scattering cannot describe the rather flat behavior predicted by state-of-the-art LQCD simulations. The disagreement is manifest from pion masses right above the physical point. This feature, earlier observed in nonrelativistic heavy-baryon ChPT [29,30], is therefore also present in the relativistic theory. The fact that $\mathcal{O}(p^4)$ terms become large from relatively low $M_\pi \gtrsim 200$ MeV implies that $\mathcal{O}(p^3)$ analyses of $g_A(M_\pi)$ likely underestimate theoretical uncertainties.

In line with the findings of Ref. [30] within heavy-baryon ChPT, we can satisfactorily describe the LQCD data

for $g_A(M_\pi)$ at $\mathcal{O}(p^4)$ only after the Δ is incorporated as an explicit degree of freedom. However, although in a much smaller degree than in the $\not{\Delta}$ case, a fast increase in the relative size of $\mathcal{O}(p^4)$ terms with M_π is observed and reflected by the estimate of theoretical uncertainties. This fact jeopardizes the precision of the ChPT description of $g_A(M_\pi)$ at $M_\pi \gtrsim 300$ MeV and negatively influences the extraction of LECs based on LQCD data at such M_π. Together with the sizable correlations, which can be reduced by considering both the M_π and q^2 dependence of the axial form factor in the fits, this feature implies that heavier resonances and/or $\mathcal{O}(p^5)$ terms are still required to reach a good convergence and reduce theoretical errors. The impact of setting the baryon masses in the loops to the values obtained by the LQCD simulations may be also worth exploring in view of the results of Ref. [35], although this would correspond to the resummation of baryon self-energy insertions of higher order. For this purpose, it would be relevant to have more information about the Δ pole position for the different lattice ensembles.

From our $\mathcal{O}(p^4)$ analysis of recent LQCD data, we have obtained $g_A(M_{\pi(\mathrm{phys})}) = 1.260 \pm 0.012$, close to the experimental value, and $d_{16} = -0.88 \pm 0.88$ GeV^{-2}, in agreement with πN phenomenology. As a consequence of the previously discussed issues, errors are still large, particularly for d_{16} that is naturally extracted from the light-quark mass dependence of the nucleon axial coupling. New LQCD results at $M_\pi \lesssim 250$ MeV will improve the precision of the extracted LECs. Besides, our ongoing effort to extend the analysis to the whole axial form factor (at low q^2) may shed more light on d_{16}, as well as other LECs such as d_{22}.

relevant information about the NME ones. This research has been partially supported by the Spanish Ministerio de Ciencia e Innovación under Contracts No. FIS2017-84038-C2-1-P and No. PID2020–112777 GB-I00, the EU STRONG-2020 project under Program No. H2020-INFRAIA-2018-1, Grant Agreement No. 824093, and by Generalitat Valenciana under Contract No. PROMETEO/2020/023.

APPENDIX A: LEC CONVERSION

The covariant renormalization prescription adopted in Refs. [25,26] differs from EOMS. In EOMS, only power-counting breaking terms are absorbed in the LECs. To obtain an equivalence between covariant and heavy-baryon results, the prescription of Ref. [25] also subtracts infrared-regular terms at the order of the calculation, as well as pieces proportional to $\log(M_\pi^2/m_N^2)$. After setting $\bar{\lambda} = 0$ and $\mu = m_N$ in Eq. (21) of Ref. [25], one is left with a dimensionally regularized LEC, x_r,

$$
\begin{aligned}
x_r &= \bar{x}^{\mathrm{cov}} + \frac{1}{F_\pi^2}(\delta\bar{x}_f^{(3)} + \delta\bar{x}_f^{(4)}) + \frac{\beta_x}{32\pi^2 F_\pi^2}\log\left(\frac{M_{\pi(\mathrm{phys})}^2}{m_{N(\mathrm{phys})}^2}\right) \\
&= x^{\mathrm{EOMS}} + \delta x_f^{\mathrm{EOMS}}, \quad\quad\quad\quad\quad\quad\quad\quad\quad (\mathrm{A1})
\end{aligned}
$$

which allows one to express the renormalized EOMS LECs x^{EOMS} in terms of the corresponding ones, $\bar{x}^{\mathrm{cov}}$, from Refs. [25,26]. The β-functions β_x required to cancel the mesonic tadpole terms are listed in Appendix B of Ref. [25] as well as finite shifts $\delta\bar{x}_f^{(3,4)}$. Our EOMS finite shifts $\delta x_f^{\mathrm{EOMS}}$ are given in the supplementary material [46]. In particular, for the relevant LECs in this study, we obtain that

$$
d_{16}^{\mathrm{EOMS}} = d_{16}^{\mathrm{cov}} + \frac{1}{F_\pi^2}\delta\bar{d}_{16f}^{(3)} + \frac{\beta_{d_{16}}}{32\pi^2 F_\pi^2}\log\left(\frac{M_{\pi(\mathrm{phys})}^2}{m_{N(\mathrm{phys})}^2}\right), \quad (\mathrm{A2})
$$

with

$$
\delta\bar{d}_{16f}^{(3)} = \frac{1}{32\pi^2}(\overset{\circ}{g}_A + \overset{\circ}{g}_A^3) \quad \text{and} \quad \beta_{d_{16}} = \frac{\overset{\circ}{g}_A}{2} + \overset{\circ}{g}_A^3 \quad (\mathrm{A3})
$$

because, in this case, $\delta\bar{d}_{16f}^{(4)} = \delta d_{16f}^{\mathrm{EOMS}}$. Furthermore,

$$
c_{1-4}^{\mathrm{EOMS}} = c_{1-4}^{\mathrm{cov}} \quad\quad\quad\quad\quad (\mathrm{A4})
$$

once $\beta_{c_{1-4}} = 0$ [25], and the finite shifts coincide with those in EOMS. Equations (A2)–(A4) are derived for the $\Delta\!\!\!/$ case but hold also for the model with the Δ pole of Ref. [25] as it does not involve additional renormalizations.

APPENDIX B: CONTRIBUTION TO g_A FROM WAVE-FUNCTION RENORMALIZATION

To the order of the present study, Z_N, defined in Eq. (8), can be written as $Z_N = 1 + \frac{1}{16\pi^2 F_\pi^2}(\delta Z_N^{(3)\mathrm{loop}} + \delta Z_N^{(4)\mathrm{loop}})$. The contribution to g_A that starts at $\mathcal{O}(p^4)$ is then $\overset{\circ}{g}_A\delta Z_N^{(4)\mathrm{loop}}$, with $\delta Z_N^{(4)\mathrm{loop}}$, including Δ, given by

$$
\begin{aligned}
\delta Z_N^{(4)\mathrm{loop}} = &-\frac{24c_1\overset{\circ}{g}_A^2 M_\pi^5 f(M_\pi)}{\overset{\circ}{m}^3 a^{3/2}}\{6\overset{\circ}{m}^4 - 6M_\pi^2\overset{\circ}{m}^2 + M_\pi^4\} \\
&+ \frac{2M_\pi^4}{27\overset{\circ}{m}^3}\left\{ \frac{a_1 h_A^2 \overset{\circ}{m}}{\overset{\circ}{m}_\Delta^4}(18\overset{\circ}{m}^4\overset{\circ}{m}_\Delta - 4\overset{\circ}{m}^3(M_\pi^2 - 9\overset{\circ}{m}_\Delta^2) + \overset{\circ}{m}^2(36\overset{\circ}{m}_\Delta^3 - 103M_\pi^2\overset{\circ}{m}_\Delta) - 36\overset{\circ}{m}\overset{\circ}{m}_\Delta^2(M_\pi^2 + 4\overset{\circ}{m}_\Delta^2) \right. \\
&+ 54\overset{\circ}{m}_\Delta(M_\pi^4 + M_\pi^2\overset{\circ}{m}_\Delta^2 - 5\overset{\circ}{m}_\Delta^4)) + \frac{18c_1}{\overset{\circ}{m}_\Delta^2}\left(\frac{18\overset{\circ}{g}_A^2\overset{\circ}{m}^2\overset{\circ}{m}_\Delta^2(M_\pi^2 - 2\overset{\circ}{m}^2)}{a} + h_A^2(8\overset{\circ}{m}^4 + 6\overset{\circ}{m}^3\overset{\circ}{m}_\Delta \right. \\
&\left. \left. + \overset{\circ}{m}^2(M_\pi^2 - 2\overset{\circ}{m}_\Delta^2)6\overset{\circ}{m}\overset{\circ}{m}_\Delta(M_\pi^2 - 2\overset{\circ}{m}_\Delta^2) - 6(M_\pi^4 - 3M_\pi^2\overset{\circ}{m}_\Delta^2 + 3\overset{\circ}{m}_\Delta^4)) \right) \right\} \\
&+ \frac{4M_\pi^4}{9\overset{\circ}{m}^3\overset{\circ}{m}_\Delta^4}\log\left(\frac{\overset{\circ}{m}^2}{M_\pi^2}\right)\{a_1 h_A^2\overset{\circ}{m}(-9\overset{\circ}{m}^4\overset{\circ}{m}_\Delta + \overset{\circ}{m}^3(4M_\pi^2 - 6\overset{\circ}{m}_\Delta^2) + 13\overset{\circ}{m}^2 M_\pi^2\overset{\circ}{m}_\Delta - 3M_\pi^4\overset{\circ}{m}_\Delta + 3\overset{\circ}{m}_\Delta^5) \\
&- 27c_1 g^2\overset{\circ}{m}_\Delta^4 M_\pi^2\} \\
&+ \frac{8}{3}h_A^2 M_\pi^2\log(\overset{\circ}{m})\left\{a_1\left(\frac{2\overset{\circ}{m}_\Delta^3}{\overset{\circ}{m}^2} - 2\overset{\circ}{m} + \overset{\circ}{m}_\Delta\right) - \frac{6c_1 M_\pi^2(2\overset{\circ}{m} + \overset{\circ}{m}_\Delta)}{\overset{\circ}{m}_\Delta^2}\right\} \\
&- \frac{8c_1 h_A^2 M_\pi^2\log(M_\pi)}{3\overset{\circ}{m}^5\overset{\circ}{m}_\Delta^2}\{5\overset{\circ}{m}^8 + 6\overset{\circ}{m}^7\overset{\circ}{m}_\Delta - 3\overset{\circ}{m}^6(2M_\pi^2 + \overset{\circ}{m}_\Delta^2) - 3\overset{\circ}{m}^5\overset{\circ}{m}_\Delta(M_\pi^2 + \overset{\circ}{m}_\Delta^2) \\
&+ \overset{\circ}{m}^2(2M_\pi^6 - 3M_\pi^4\overset{\circ}{m}_\Delta^2 + \overset{\circ}{m}_\Delta^6) + 3\overset{\circ}{m}\overset{\circ}{m}_\Delta(M_\pi^2 - \overset{\circ}{m}_\Delta^2)^3 - 3(M_\pi^2 - \overset{\circ}{m}_\Delta^2)^4\}
\end{aligned}
$$

$$-\frac{4a_1 h_A^2 M_\pi^2}{3\mathring{m}^2 \mathring{m}_\Delta^3}\log\left(\frac{\mathring{m}^2}{\mathring{m}_\Delta^2}\right)\{9\mathring{m}^4 M_\pi^2 + \mathring{m}^3(4M_\pi^2\mathring{m}_\Delta - 2\mathring{m}_\Delta^3) + \mathring{m}^2(\mathring{m}_\Delta^4 - 3M_\pi^4) - M_\pi^6 + M_\pi^2\mathring{m}_\Delta^4 + 2\mathring{m}_\Delta^6\}$$

$$+\frac{2a_1 h_A^2 M_\pi^2}{3\mathring{m}^4 \mathring{m}_\Delta^3}\log\left(\frac{M_\pi^2}{\mathring{m}_\Delta^2}\right)\{-5\mathring{m}^8 - 4\mathring{m}^7\mathring{m}_\Delta + 6\mathring{m}^6 M_\pi^2 + 2\mathring{m}^5\mathring{m}_\Delta(M_\pi^2 - 3\mathring{m}_\Delta^2)$$

$$+ 2\mathring{m}^2(M_\pi^6 + M_\pi^2\mathring{m}_\Delta^4 - 2\mathring{m}_\Delta^6) + 2\mathring{m}\mathring{m}_\Delta(M_\pi^2 - \mathring{m}_\Delta^2)^2(M_\pi^2 + 5\mathring{m}_\Delta^2) - 3(M_\pi^2 - \mathring{m}_\Delta^2)^3(M_\pi^2 + 3\mathring{m}_\Delta^2)\}$$

$$-\frac{8h_A^2 M_\pi^2}{3\mathring{m}^5 \mathring{m}_\Delta^3}\log(\mathring{m}_\Delta)\{a_1\mathring{m}(5\mathring{m}^8 + 4\mathring{m}^7\mathring{m}_\Delta + 4\mathring{m}^5\mathring{m}_\Delta^3 + \mathring{m}^4\mathring{m}_\Delta^4 + 6\mathring{m}^2\mathring{m}_\Delta^6 - 10\mathring{m}\mathring{m}_\Delta^7 - 9\mathring{m}_\Delta^8)$$

$$- c_1\mathring{m}_\Delta(-5\mathring{m}^8 - 6\mathring{m}^7\mathring{m}_\Delta + 3\mathring{m}^6(2M_\pi^2 + \mathring{m}_\Delta^2) + 3\mathring{m}^5\mathring{m}_\Delta(M_\pi^2 + \mathring{m}_\Delta^2) + \mathring{m}^2(2M_\pi^6 - 3M_\pi^4\mathring{m}_\Delta^2 - \mathring{m}_\Delta^6)$$

$$+ 3\mathring{m}\mathring{m}_\Delta(M_\pi^6 - 3M_\pi^4\mathring{m}_\Delta^2 + 3M_\pi^2\mathring{m}_\Delta^4 + \mathring{m}_\Delta^6) - 3(M_\pi^8 - 4M_\pi^6\mathring{m}_\Delta^2 + 6M_\pi^4\mathring{m}_\Delta^4 - 4M_\pi^2\mathring{m}_\Delta^6 - \mathring{m}_\Delta^8))\}$$

$$+\frac{4h_A^2 M_\pi^2(\mathring{m} - \mathring{m}_\Delta)(\mathring{m} + \mathring{m}_\Delta)^3}{3\mathring{m}^5 \mathring{m}_\Delta^3}\log(\mathring{m}_\Delta^2 - \mathring{m}^2)\{a_1\mathring{m}(5\mathring{m}^4 - 6\mathring{m}^3\mathring{m}_\Delta + 12\mathring{m}^2\mathring{m}_\Delta^2 - 8\mathring{m}\mathring{m}_\Delta^3 + 9\mathring{m}_\Delta^4)$$

$$+ 2c_1\mathring{m}_\Delta(5\mathring{m}^4 - 4\mathring{m}^3\mathring{m}_\Delta + 5\mathring{m}^2\mathring{m}_\Delta^2 - 3\mathring{m}\mathring{m}_\Delta^3 + 3\mathring{m}_\Delta^4)\}$$

$$+\frac{F(M_\pi)}{3\mathring{m}^5 \mathring{m}_\Delta^3}\{4h_A^2(\mathring{m}^2 + 2\mathring{m}\mathring{m}_\Delta - M_\pi^2 + \mathring{m}_\Delta^2)(a_1\mathring{m}(5\mathring{m}^8 - 6\mathring{m}^7\mathring{m}_\Delta + 2\mathring{m}^6(\mathring{m}_\Delta^2 - 6M_\pi^2)$$

$$+ 4\mathring{m}^5(2M_\pi^2\mathring{m}_\Delta + \mathring{m}_\Delta^3) + 2\mathring{m}^4(3M_\pi^4 - 5\mathring{m}_\Delta^4) + 2\mathring{m}^3\mathring{m}_\Delta(M_\pi^4 - 6M_\pi^2\mathring{m}_\Delta^2 + 5\mathring{m}_\Delta^4)$$

$$+ \mathring{m}^2(4M_\pi^6 - 2M_\pi^4\mathring{m}_\Delta^2 + 4M_\pi^2\mathring{m}_\Delta^4 - 6\mathring{m}_\Delta^6) - 4\mathring{m}(M_\pi^6\mathring{m}_\Delta - 3M_\pi^2\mathring{m}_\Delta^5 + 2\mathring{m}_\Delta^7)$$

$$- 3(M_\pi^2 - \mathring{m}_\Delta^2)^3(M_\pi^2 + 3\mathring{m}_\Delta^2))$$

$$+ 2c_1\mathring{m}_\Delta(5\mathring{m}^8 - 4\mathring{m}^7\mathring{m}_\Delta - \mathring{m}^6(6M_\pi^2 + 5\mathring{m}_\Delta^2) + \mathring{m}^5(5\mathring{m}_\Delta^3 - M_\pi^2\mathring{m}_\Delta) + 2\mathring{m}^4\mathring{m}_\Delta^2(M_\pi^2 - \mathring{m}_\Delta^2)$$

$$+ 2\mathring{m}^3\mathring{m}_\Delta(M_\pi^2 - \mathring{m}_\Delta^2)^2 - \mathring{m}^2(2M_\pi^6 - 3M_\pi^4\mathring{m}_\Delta^2 + \mathring{m}_\Delta^6) + 3\mathring{m}\mathring{m}_\Delta(M_\pi^2 - \mathring{m}_\Delta^2)^3 + 3(M_\pi^2 - \mathring{m}_\Delta^2)^4))\}, \tag{B1}$$

with the following definitions:

$$F(M_\pi) \equiv \frac{M_\pi^2}{b}\log\left(\frac{-\mathring{m}^2 + b + M_\pi^2 + \mathring{m}_\Delta^2}{2M_\pi\mathring{m}_\Delta}\right), \qquad f(M_\pi) \equiv i\log\left(\frac{M_\pi + i\sqrt{a}}{2\mathring{m}}\right), \tag{B2}$$

where $b \equiv \sqrt{\mathring{m}^4 - 2\mathring{m}^2(M_\pi^2 + \mathring{m}_\Delta^2) + (M_\pi^2 - \mathring{m}_\Delta^2)^2}$, and $a \equiv 4\mathring{m}^2 - M_\pi^2$. This result, but also the full expression for the $\mathcal{O}(p^4)$ nucleon self-energy Σ_N with explicit Δ, from which Z_N is derived using Eq. (8), can be found in the Mathematica notebook provided as supplementary material [46].

[1] M. Gorchtein and C.-Y. Seng, Dispersion relation analysis of the radiative corrections to g_A in the neutron β-decay, J. High Energy Phys. 10 (**2021**) 053.

[2] P. Zyla et al. (Particle Data Group), Review of particle physics, Prog. Theor. Exp. Phys. **2020**, 083C01 (2020).

[3] H.-W. Lin, Frontiers in lattice nucleon structure, Int. J. Mod. Phys. A **35**, 2030006 (2020).

[4] Y. Aoki et al., FLAG review 2021, arXiv:2111.09849.

[5] B. C. Tiburzi, Time dependence of nucleon correlation functions in chiral perturbation theory, Phys. Rev. D **80**, 014002 (2009).

[6] O. Bar, Chiral perturbation theory and nucleon–pion-state contaminations in lattice QCD, Int. J. Mod. Phys. A **32**, 1730011 (2017).

[7] S. R. Beane and M. J. Savage, Nucleon properties at finite lattice spacing in chiral perturbation theory, Phys. Rev. D **68**, 114502 (2003).

[8] S. R. Beane and M. J. Savage, Baryon axial charge in a finite volume, Phys. Rev. D **70,** 074029 (2004).

[9] G. S. Bali, L. Barca, S. Collins, M. Gruber, M. Löffler, A. Schäfer, W. Söldner, P. Wein, S. Weishäupl, and T. Wurm (RQCD Collaboration), Nucleon axial structure from lattice QCD, J. High Energy Phys. 05 (2020) 126.

[10] S. R. Beane and M. J. Savage, The Quark mass dependence of two nucleon systems, Nucl. Phys. **A717,** 91 (2003).

[11] J. C. Berengut, E. Epelbaum, V. V. Flambaum, C. Hanhart, U. G. Meissner, J. Nebreda, and J. R. Pelaez, Varying the light quark mass: Impact on the nuclear force and Big Bang nucleosynthesis, Phys. Rev. D **87,** 085018 (2013).

[12] E. Epelbaum, H. Krebs, T. A. Lähde, D. Lee, and U.-G. Meißner, Dependence of the triple-alpha process on the fundamental constants of nature, Eur. Phys. J. A **49,** 82 (2013).

[13] V. Bernard, N. Kaiser, T. S. H. Lee, and U.-G. Meissner, Threshold pion electroproduction in chiral perturbation theory, Phys. Rep. **246,** 315 (1994).

[14] M. Hilt, B. C. Lehnhart, S. Scherer, and L. Tiator, Pion photo- and electroproduction in relativistic baryon chiral perturbation theory and the chiral MAID interface, Phys. Rev. C **88,** 055207 (2013).

[15] G. H. Guerrero Navarro and M. J. Vicente Vacas, Threshold pion electro- and photoproduction off nucleons in covariant chiral perturbation theory, Phys. Rev. D **102,** 113016 (2020).

[16] N. Rijneveen, A. M. Gasparyan, H. Krebs, and E. Epelbaum, Pion photoproduction in chiral perturbation theory with explicit treatment of the $\Delta(1232)$ resonance, arXiv:2108.01619.

[17] M. Mojzis, Elastic pi N scattering to O(p**3) in heavy baryon chiral perturbation theory, Eur. Phys. J. C **2,** 181 (1998).

[18] N. Fettes and U.-G. Meissner, Pion nucleon scattering in chiral perturbation theory. 2.: Fourth order calculation, Nucl. Phys. **A676,** 311 (2000).

[19] N. Fettes and U. G. Meissner, Pion—nucleon scattering in an effective chiral field theory with explicit spin 3/2 fields, Nucl. Phys. **A679,** 629 (2001).

[20] K. Torikoshi and P. J. Ellis, Low-energy pion nucleon scattering in the heavy baryon and infrared schemes, Phys. Rev. C **67,** 015208 (2003).

[21] M. Hoferichter, J. Ruiz de Elvira, B. Kubis, and U.-G. Meißner, Roy–Steiner-equation analysis of pion–nucleon scattering, Phys. Rep. **625,** 1 (2016).

[22] Y.-H. Chen, D.-L. Yao, and H. Q. Zheng, Analyses of pion-nucleon elastic scattering amplitudes up to $O(p^4)$ in extended-on-mass-shell subtraction scheme, Phys. Rev. D **87,** 054019 (2013).

[23] J. M. Alarcon, J. Martin Camalich, and J. A. Oller, Improved description of the πN-scattering phenomenology in covariant baryon chiral perturbation theory, Ann. Phys. (Amsterdam) **336,** 413 (2013).

[24] D.-L. Yao, D. Siemens, V. Bernard, E. Epelbaum, A. M. Gasparyan, J. Gegelia, H. Krebs, and U.-G. Meißner, Pion-nucleon scattering in covariant baryon chiral perturbation theory with explicit Delta resonances, J. High Energy Phys. 05 (2016) 038.

[25] D. Siemens, V. Bernard, E. Epelbaum, A. Gasparyan, H. Krebs, and U.-G. Meißner, Elastic pion-nucleon scattering in chiral perturbation theory: A fresh look, Phys. Rev. C **94,** 014620 (2016).

[26] D. Siemens, V. Bernard, E. Epelbaum, A. M. Gasparyan, H. Krebs, and U.-G. Meißner, Elastic and inelastic pion-nucleon scattering to fourth order in chiral perturbation theory, Phys. Rev. C **96,** 055205 (2017).

[27] J. Kambor and M. Mojzis, Field redefinitions and wave function renormalization to O(p**4) in heavy baryon chiral perturbation theory, J. High Energy Phys. 04 (1999) 031.

[28] T. R. Hemmert, M. Procura, and W. Weise, Quark mass dependence of the nucleon axial vector coupling constant, Phys. Rev. D **68,** 075009 (2003).

[29] V. Bernard and U.-G. Meissner, The Nucleon axial-vector coupling beyond one loop, Phys. Lett. B **639,** 278 (2006).

[30] M. Procura, B. U. Musch, T. R. Hemmert, and W. Weise, Chiral extrapolation of g(A) with explicit Delta(1232) degrees of freedom, Phys. Rev. D **75,** 014503 (2007).

[31] A. Calle Cordon and J. L. Goity, Baryon masses and axial couplings in the combined $1/N_c$ and chiral expansions, Phys. Rev. D **87,** 016019 (2013).

[32] M. R. Schindler, T. Fuchs, J. Gegelia, and S. Scherer, Axial, induced pseudoscalar, and pion-nucleon form-factors in manifestly Lorentz-invariant chiral perturbation theory, Phys. Rev. C **75,** 025202 (2007).

[33] S.-i. Ando and H. W. Fearing, Ordinary muon capture on a proton in manifestly Lorentz invariant baryon chiral perturbation theory, Phys. Rev. D **75,** 014025 (2007).

[34] D.-L. Yao, L. Alvarez-Ruso, and M. J. Vicente-Vacas, Extraction of nucleon axial charge and radius from lattice QCD results using baryon chiral perturbation theory, Phys. Rev. D **96,** 116022 (2017).

[35] M. F. M. Lutz, U. Sauerwein, and R. G. E. Timmermans, On the axial-vector form factor of the nucleon and chiral symmetry, Eur. Phys. J. C **80,** 844 (2020).

[36] S. Weinberg, Effective chiral Lagrangians for nucleon—pion interactions and nuclear forces, Nucl. Phys. **B363,** 3 (1991).

[37] T. R. Hemmert, B. R. Holstein, and J. Kambor, Systematic 1/M expansion for spin 3/2 particles in baryon chiral perturbation theory, Phys. Lett. B **395,** 89 (1997).

[38] T. R. Hemmert, B. R. Holstein, and J. Kambor, Chiral Lagrangians and delta(1232) interactions: Formalism, J. Phys. G **24,** 1831 (1998).

[39] N. Fettes, U.-G. Meissner, M. Mojzis, and S. Steininger, The Chiral effective pion nucleon Lagrangian of order p**4, Ann. Phys. (Amsterdam)**283,** 273 (2000); **288,** 249(E) (2001).

[40] S.-Z. Jiang, Y.-R. Liu, and H.-Q. Wang, Chiral Lagrangians with $\Delta(1232)$ to one loop, Phys. Rev. D **97,** 014002 (2018).

[41] M. Holmberg and S. Leupold, The relativistic chiral Lagrangian for decuplet and octet baryons at next-to-leading order, Eur. Phys. J. A **54,** 103 (2018).

[42] Y. Ünal, A. Küçükarslan, and S. Scherer, Axial-vector nucleon-to-delta transition form factors using the complex-mass renormalization scheme, Phys. Rev. D **104,** 094014 (2021).

[43] C. Hacker, N. Wies, J. Gegelia, and S. Scherer, Including the Delta(1232) resonance in baryon chiral perturbation theory, Phys. Rev. C **72**, 055203 (2005).

[44] D. Siemens, Elastic pion-nucleon scattering in chiral perturbation theory: Explicit $\Delta(1232)$ degrees of freedom, arXiv:2001.03906.

[45] T. Fuchs, J. Gegelia, G. Japaridze, and S. Scherer, Renormalization of relativistic baryon chiral perturbation theory and power counting, Phys. Rev. D **68**, 056005 (2003).

[46] See Supplemental Material at http://link.aps.org/supplemental/10.1103/PhysRevD.105.074001 for *Mathematica* expressions.

[47] C. C. Chang *et al.*, A per-cent-level determination of the nucleon axial coupling from quantum chromodynamics, Nature (London) **558**, 91 (2018).

[48] T. Harris, G. von Hippel, P. Junnarkar, H. B. Meyer, K. Ottnad, J. Wilhelm, H. Wittig, and L. Wrang, Nucleon isovector charges and twist-2 matrix elements with $N_f = 2 + 1$ dynamical Wilson quarks, Phys. Rev. D **100**, 034513 (2019).

[49] S. Park, R. Gupta, B. Yoon, S. Mondal, T. Bhattacharya, Y.-C. Jang, B. Joó, and F. Winter (Nucleon Matrix Elements (NME) Collaboration), Precision nucleon charges and form factors using $2 + 1$-flavor lattice QCD, Phys. Rev. D **105**, 054505 (2022).

[50] M. Constantinou, Lattice generalized parton distributions and form factors of the nucleon, in *Proceedings of the 22nd International Symposium on Spin Physics* (2017), arXiv:1701.02855.

[51] S. Wesolowski, N. Klco, R. J. Furnstahl, D. R. Phillips, and A. Thapaliya, Bayesian parameter estimation for effective field theories, J. Phys. G **43**, 074001 (2016).

[52] A. Manohar and H. Georgi, Chiral quarks and the non-relativistic quark model, Nucl. Phys. **B234**, 189 (1984).

[53] S. Scherer and M. R. Schindler, *A Primer for Chiral Perturbation Theory*, Lecture Notes in Physics Vol. 830 (Springer, Berlin, Heidelberg, 2012), 10.1007/978-3-642-19254-8.

[54] E. Epelbaum, H. Krebs, and U. G. Meißner, Improved chiral nucleon-nucleon potential up to next-to-next-to-next-to-leading order, Eur. Phys. J. A **51**, 53 (2015).

[55] R. J. Furnstahl, N. Klco, D. R. Phillips, and S. Wesolowski, Quantifying truncation errors in effective field theory, Phys. Rev. C **92**, 024005 (2015).

[56] S. L. Adler, Calculation of the Axial Vector Coupling Constant Renormalization in Beta Decay, Phys. Rev. Lett. **14**, 1051 (1965).

[57] W. I. Weisberger, Renormalization of the Weak Axial Vector Coupling Constant, Phys. Rev. Lett. **14**, 1047 (1965).

[58] L. Alvarez-Ruso, T. Ledwig, J. Martin Camalich, and M. J. Vicente-Vacas, Nucleon mass and pion-nucleon sigma term from a chiral analysis of lattice QCD data, Phys. Rev. D **88**, 054507 (2013).